Progress In Electromagnetics Research M, Vol. 26, 205–223, 2012

PERMANENT MAGNET BEARINGS: ANALYSIS OF PLANE AND AXISYMMETRIC V-SHAPED ELEMENT DESIGN

F. Di Puccio[1], R. Bassani[1], E. Ciulli[1], A. Musolino[2, *], and R. Rizzo[2]

[1]Department of Mechanical, Nuclear and Industrial Engineering, University of Pisa, Via Diotisalvi 2, Pisa 56126, Italy

[2]Department of Energy and System Engineering, University of Pisa, Via Diotisalvi 2, Pisa 56126, Italy

Abstract—Applications of permanent magnets bearings have gained a new interest thanks to the development of rare earth materials, characterised by residual magnetic induction greater than 1 T. The present paper proposes a new geometry for permanent magnets bearings with V-shaped elements, both for a plane slide and for cylindrical bearings. The aim of this geometry is to give new possibilities to the application of these bearing systems, by reducing its inherent instability. A design method, involving Finite Elements and Magnetic Field Integral Equations analyses, is also described for defining the most suitable V-opening angle and the two magnetisation directions. These parameters can be varied in order to reduce the unstable force in the coupling, and to reach the desired force and stiffness in the stable direction. The design is founded on the evaluation of four "geometric" vectors, that depend on the geometry of the elements. Some results are reported for a reference geometry for both the slide and the cylindrical bearings.

1. INTRODUCTION

Permanent magnets are a fascinating solution in applications where friction and wear are the main causes of damage and even of failure. In fact, since magnetic levitation causes no contact, magnet bearings are efficiently employed in high speed systems and in cases where no contamination is required [1–3]. On the other side, the use

Received 14 September 2012, Accepted 12 October 2012, Scheduled 19 October 2012

* Corresponding author: Antonino Musolino (musolino@dsea.unipi.it).

of permanent magnets has been limited in the past because of the low forces they generate and because of the instability of the coupling. The limit on the low forces has been enhanced by rare earths materials, which show residual magnetic induction B_R greater than 1 T [4, 5]. The question of instability can be faced in different ways, e.g., by introducing an active control or diamagnetic elements or superconductors. In addition the element shapes and the field directions can be conveniently modified in order to reduce the unstable force [6]. In this way, although the question of instability is not completely solved, the control system can be prompter and more reliable. A new geometry with a V section, defined by an angle α is proposed, with arbitrary generic magnetisation directions on the inner and outer elements (Figure 1). Such a geometry may offer advantageous configurations with respect to the most common passive bearing solutions limited to rectangular/annular shapes with axial and radial magnetisations [7–14].

2. THEORETICAL BACKGROUND

The investigation of the new V-shaped geometry requires some preliminary considerations about the equilibrium and the methods for evaluating forces. As shown in Figure 1, it is possible to define M_I and M_E as the magnetisation vectors of the permanent magnets that constitute the internal and external elements of the bearing, respectively. θ_I and θ_E are their orientations with respect to the vertical (z-axis) direction.

2.1. Equilibrium in Magnetostatics

In Magnetostatics the possibility of a stable equilibrium of a configuration with permanent magnets is definitely excluded by

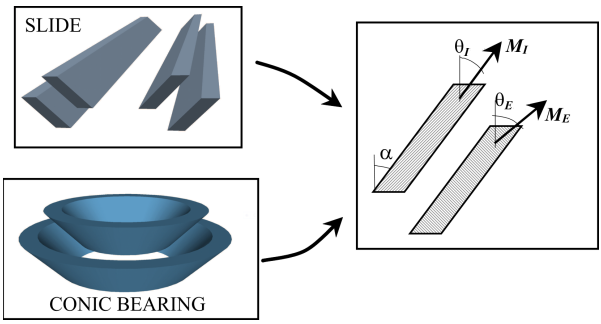

Figure 1. V-shaped magnetic bearings.

Earnshaw's theorem (1842) [15]. In fact, although it may be possible to find a point where the total force and total torque are zero, such an equilibrium is always unstable in one or more directions. As already known, the condition of stability in the direction n is given by the negativeness of the derivative of the force n-th component with respect to the displacement in that direction, i.e., $\partial F_n/\partial x_n < 0$.

As a consequence of the Laplace equation governing steady magnetic systems, it could be proved that when $\mu_R > 1$ and $\mu_R = 1$ the following relations respectively hold [16]:

$$\begin{aligned} \frac{\partial F_x}{\partial x} + \frac{\partial F_y}{\partial y} + \frac{\partial F_z}{\partial z} &> 0 \\ \frac{\partial F_x}{\partial x} + \frac{\partial F_y}{\partial y} + \frac{\partial F_z}{\partial z} &= 0 \end{aligned} \tag{1}$$

confirming Earnshaws theorem, since at least one term of the sum has to be positive. On the other side, stable equilibrium configurations exist for diamagnetic materials ($\mu_R < 1$), and for superconductors ($\mu_R = 0$), for which

$$\frac{\partial F_x}{\partial x} + \frac{\partial F_y}{\partial y} + \frac{\partial F_z}{\partial z} < 0 \tag{2}$$

Rare earth materials have a nearly unitary relative permeability (slightly > 1), therefore their use requires a compensation for the instability of the equilibrium of forces, e.g., by adding feedback control loops.

2.2. Force Evaluation

The evaluation of the forces has been carried out in accordance with the equivalent currents method [17, 18]. In the hypothesis of uniform magnetisation, which can be conveniently assumed for rare earth materials, only surface equivalent magnetization currents $\mathbf{j}_S$ are non zero:

$$\mathbf{j}_S = \mathbf{M} \times \mathbf{n} \tag{3}$$

In fact, as $\mathbf{M}$ is uniform, there is no volume current density:

$$\mathbf{j}_V = \nabla \times \mathbf{M} = 0 \tag{4}$$

According to Laplace's law the force that acts between two coils (Figure 2) is given by

$$\mathbf{F}_2 = -\mathbf{F}_1 = -\frac{\mu_0 j_1 j_2}{4\pi} \iint \frac{\mathbf{r}(d\mathbf{s}_1 \cdot d\mathbf{s}_2)}{r^3} \tag{5}$$

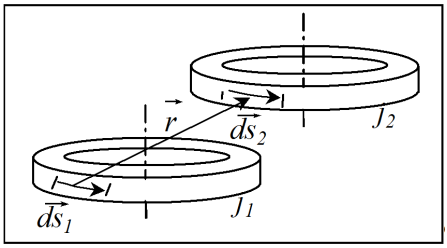

Figure 2. Force between two coils: symbols in (5).

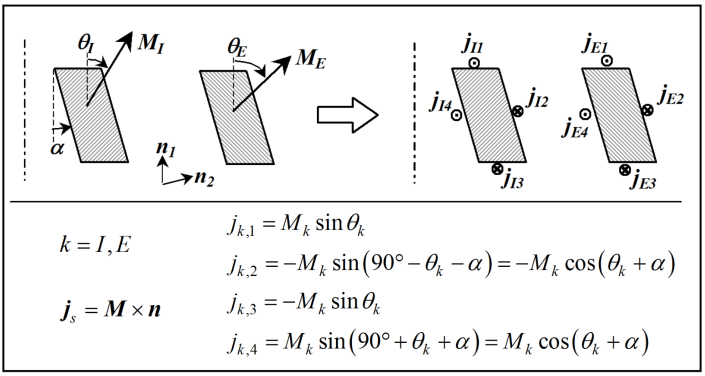

Figure 3. V-shaped magnets: equivalent surface current densities.

For the V-shaped elements, the resultant force **F** between the two parts can thus be obtained as sum of the effects of the interactions of each current of the inner part with the four currents of the outer one. In Figure 3, only half section is shown, cause sections and magnetisations are supposed to be symmetric.

By the application of (5) to the V-shape, a total of 16 integrals come out, that can be gathered in four groups, each one depending on the magnetisations $\mathbf{M}_I$ and $\mathbf{M}_E$ and on the geometry through four geometric vectors $\mathbf{A}_i$:

$$\mathbf{F}_E = -\mathbf{F}_I = \frac{\mu_0 M_I M_E}{4\pi}\Big[\sin\theta_I \sin\theta_E \mathbf{A}_1 + \sin\theta_I \cos(\alpha+\theta_E)\mathbf{A}_2 + \sin\theta_E \cos(\alpha+\theta_I)\mathbf{A}_3 + \cos(\alpha+\theta_I)\cos(\alpha+\theta_E)\mathbf{A}_4\Big] \quad (6)$$

As shown in (6) the influence of the magnetisation angles is defined by trigonometric coefficients that multiply the geometric vectors [19]. Thus, once such vectors are known, the influence of the magnetisation direction of $\mathbf{M}_I$ and $\mathbf{M}_E$ can be studied in detail. For instance the

most suitable directions for achieving the desired force and stiffness can be evaluated. Such design problem requires the knowledge of the geometric vectors, whose expressions are of the kind reported for $\mathbf{A}_1$ in (7) (see Figure 3 for symbols).

$$\begin{aligned}\mathbf{A}_1 = & \int_{I,1}\int_{E,1}\frac{\mathbf{r}(d\mathbf{s}_1\cdot d\mathbf{s}_2)}{r^3}+\int_{I,1}\int_{E,3}\frac{\mathbf{r}(d\mathbf{s}_1\cdot d\mathbf{s}_2)}{r^3}\\ & +\int_{I,3}\int_{E,1}\frac{\mathbf{r}(d\mathbf{s}_1\cdot d\mathbf{s}_2)}{r^3}+\int_{I,3}\int_{E,3}\frac{\mathbf{r}(d\mathbf{s}_1\cdot d\mathbf{s}_2)}{r^3}\end{aligned} \tag{7}$$

The expressions for $\mathbf{A}_2$, $\mathbf{A}_3$ and $\mathbf{A}_4$ have the same form; only the integration domains change:

$$\begin{aligned}\mathbf{A}_2 &= \int_{I,1}\int_{E,2}(\cdot)+\int_{I,1}\int_{E,4}(\cdot)+\int_{I,3}\int_{E,2}(\cdot)+\int_{I,3}\int_{E,4}(\cdot);\\ \mathbf{A}_3 &= \int_{I,2}\int_{E,1}(\cdot)+\int_{I,2}\int_{E,3}(\cdot)+\int_{I,4}\int_{E,1}(\cdot)+\int_{I,4}\int_{E,3}(\cdot);\\ \mathbf{A}_4 &= \int_{I,2}\int_{E,2}(\cdot)+\int_{I,2}\int_{E,4}(\cdot)+\int_{I,4}\int_{E,2}(\cdot)+\int_{I,4}\int_{E,4}(\cdot);\end{aligned}$$

It is worth noting that when one magnetisation is inverted in direction, also the force results upturned. Consequently also the stable/unstable directions are reversed.

3. GEOMETRIC VECTORS EVALUATION

Two different approaches have been followed for evaluating the geometric vectors, one based on Magnetic Field Integral Equations and the other on Finite Element calculations. Both these approaches are based upon the following consideration: according to (6), when two axial magnetisations are considered ($\theta_I = \theta_E = 0°$) the force on each element depends only on $\mathbf{A}_4$. Similarly when $\theta_I = \theta_E = 90° - \alpha$ only $\mathbf{A}_1$ is involved, when $\theta_I = 90° - \alpha$, $\theta_E = 0$ the force is proportional to $\mathbf{A}_2$, and finally when to $\theta_I = 0$, $\theta_E = 90° - \alpha$ the force is proportional to $\mathbf{A}_3$. Thus, when the force can be evaluated for the four reference cases with particular magnetisation directions, it is rather simple to determine the geometric vectors. The above mentioned approaches differ in the method for evaluating the forces, as described below.

3.1. Magnetic Field Integral Equations Method

Magnetic Field Integral Equations (MFIE) are applied to a discretized representation of the bodies under examination and solved

numerically [20, 21]. The main unknown in this approach is the magnetisation in each elemental volume, which is then used in the force expression [22]. In this case the magnetisation is given, so the method affords the numerical solution of expressions as (5) by a purpose-developed software. A research computer code, developed at the School of Engineering of the University of Pisa, has been used to simulate the behavior of the proposed magnetic bearing configuration. The code is based on an integral 3-D formulation that reduces the field analysis to the analysis of an equivalent network. The active regions only (magnetic materials and current carrying conductors, if present) are discretized by using elementary volumes, and an equivalent network is built. A detailed description of the formulation is reported in [23], while in [24–26] application examples to the analysis of electromechanical devices are described.

3.2. Finite Element Method

The evaluation of the forces for the reference cases has also been obtained by Finite Element (FE) Analysis [22] by means of the Ansys code, Emag package. Two models have been defined, distinguishing the plane case by the 3D case in order to reduce time for calculations. Very fine meshes are required around the magnets in order to define correctly the magnetic induction vector **B**. Examples of the used models are shown in Figure 4, for the conic bearing in axi-symmetric position and in plane symmetry condition [27].

Considering that they follow completely different approaches, results obtained by these two methods, and by the use of 6 have shown a very good agreement, with differences lower than 6–7%.

4. PLANAR V-SHAPED SLIDES

The V-shaped geometry has been applied for defining the section of a slide (Figure 1). Since an infinite length has been supposed, the problem has been solved by a 2D analysis.

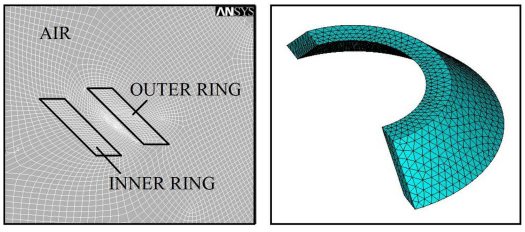

Figure 4. FE models: plane and 3D analyses for the conic bearing.

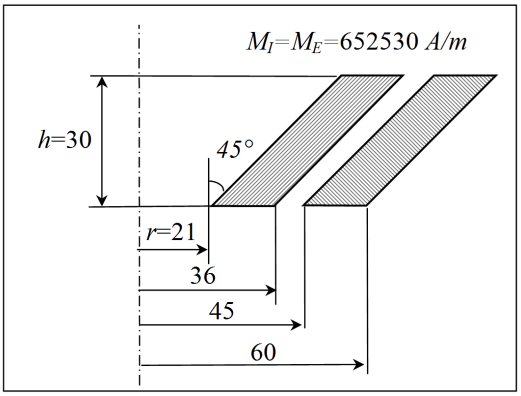

Figure 5. Reference geometry for the V-shaped slide; half section; dimensions are in millimeters.

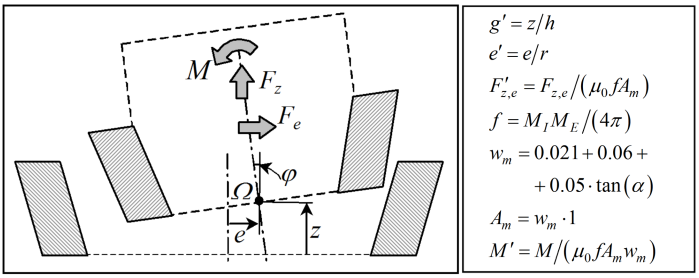

Figure 6. Definition of forces and parameters for the analysis.

4.1. Geometry

The geometry described in Figure 5 has been introduced as reference case for conducting the FE and MIE calculations. The opening angle α is posed equal to 45° and the magnitude of the magnetisations are fixed at 652530 A/m.

The force acting between the elements of the slide has been evaluated for different relative positions of the parts. Assuming as fixed the outer elements, the location of the inner elements can be identified by three degrees of freedom: the parameters e, z and φ in Figure 6 have been adopted in the present study. A simplification can be done when there are no eccentricity and rotation ($e = \varphi = 0°$), since a plane of symmetry is present and only half geometry can be considered.

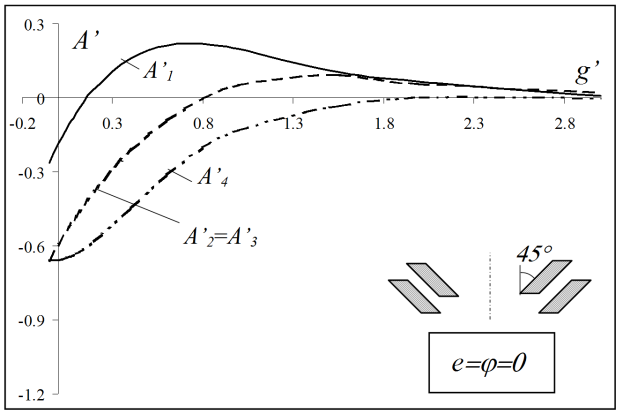

Figure 7. Dimensionless geometric vectors for symmetric slide.

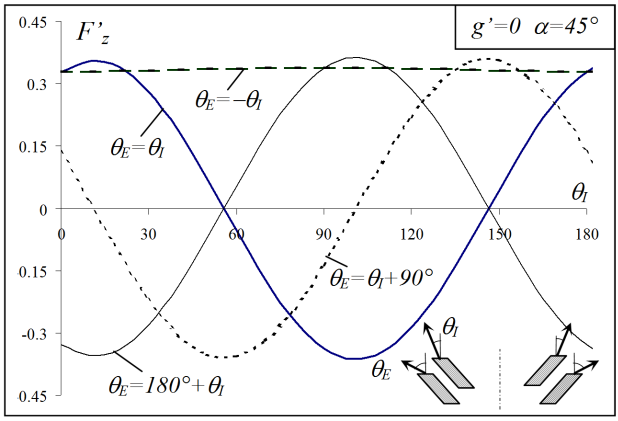

Figure 8. Dimensionless geometric vectors for symmetric slide.

4.2. Results

The first results, in dimensionless form (as defined in Figure 6 and reported to the geometry of Figure 5), are the geometric vectors in the symmetric location, where only their axial component is present. Since they have the dimensions of $[L]^2$, the geometric vectors are referred to the mean area A_m, described by a unitary length and a mean width, w_m. It is also worth noting that results are reported for the inner elements (Figure 6), those relative to the outer ones being opposite.

As shown in Figure 7, in the symmetric position and for an

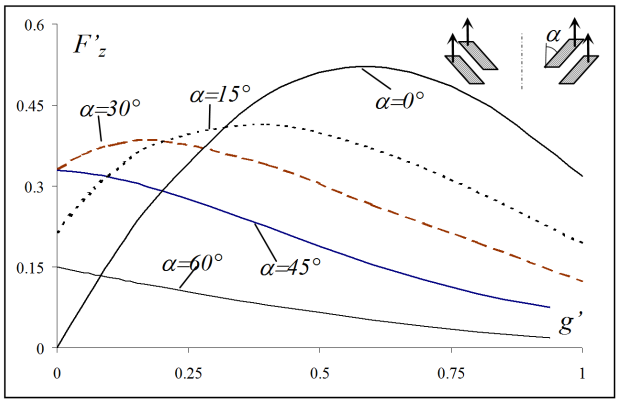

Figure 9. Dimensionless geometric vectors for symmetric slide.

opening angle of 45°, the geometric vector $\mathbf{A}_2$ is equal to $\mathbf{A}_3$. Once such geometric vectors are known, the influence of the magnetisation directions can be easily evaluated. In Figure 8 some examples for particular combinations of the magnetisation angles are reported. It can be noted that for equal magnetisations, the maximum force is obtained when $\theta_I = \theta_E = 10°$ but varies markedly with θ_I. The force remains almost constant when $\theta_I = -\theta_E$. These conditions are suitable for axial bearing applications, while an horizontally loaded system is supposed to have very low F'_z, e.g., $\theta_I = \theta_E \approx 56°$. Moreover, for $\theta_E = 180° + \theta_I$ opposite values are obtained with respect to $\theta_E = \theta_I$.

The V-shape with axial magnetizations is then varied through the angle α, as shown in Figure 9. It should be noted that all the curves in the diagram consider the same volume of permanent magnets, since the area of the section is maintained the same.

The highest force is obtained choosing the angle $\alpha = 0°$ and an axial displacement $g' \simeq 0.6$. As α grows, the maximum force is reduced in magnitude and is also shifted towards lower values of g'. The behaviour of the slide has also been investigated for different values of the eccentricity in order to determine the ratio of stable-unstable forces. Since the problem is not dependent on the length co-ordinate, the stability condition for $\mu_R = 1$ becomes:

$$\frac{\partial F_e}{\partial e} + \frac{\partial F_z}{\partial z} = 0 \tag{8}$$

Therefore the stable and the unstable directions have opposite stiffness K, $(K_n = -\partial F_n / \partial x_n)$.

According to Figure 10 the slide is stable in the z direction and

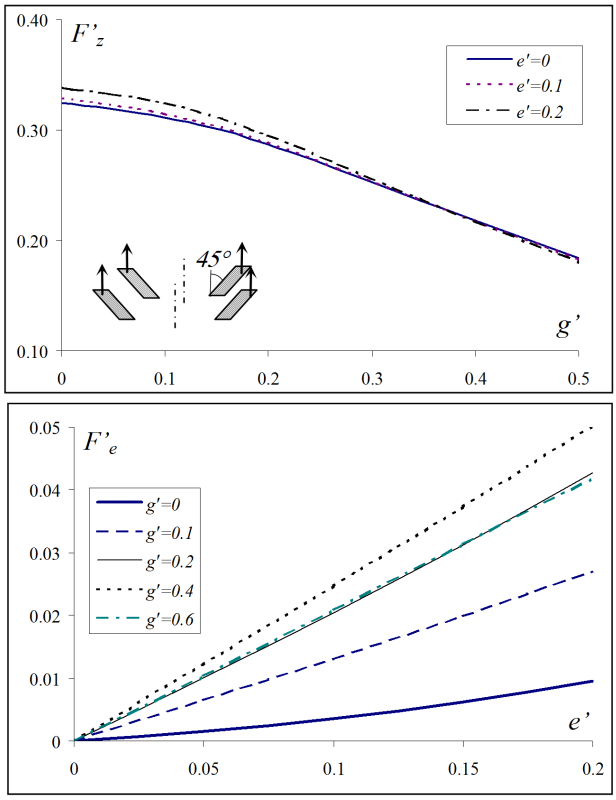

Figure 10. Dimensionless axial and transverse forces ($\alpha = 45°$, $\varphi = 0$).

unstable in the other one. It is important to underline that in the practical range of variation of e' (< 0.1) the ratio of stable/unstable force is $10 \div 20$. Another interesting effect is the presence of a tilting torque, that grows as a little eccentricity appears, even if the rotation remains equals to zero. A position of $g' = 0.5$ appears advantageous, giving $M' = 0$ for every e'.

The effect of this moment is to produce a rotation of the inner tracks. The reactive forces and moment due to this rotation are represented in Figure 12 for rather small angles. The z component of the force does not change markedly for $\varphi < 10°$ but a transverse force soon arises, which is unstable. On the other side the reactive moment has a stabilising effect. Even from these considerations a good working point is $g' \approx 0.5$.

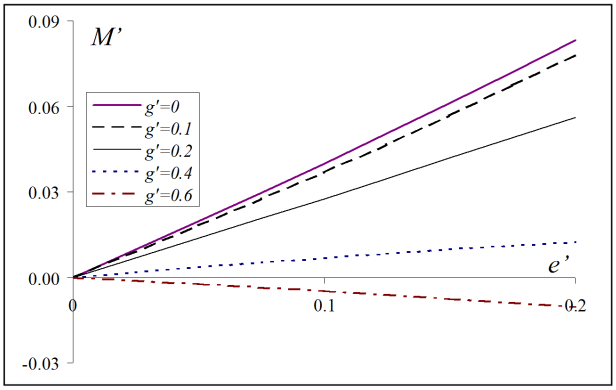

Figure 11. Dimensionless moment about point Ω ($\alpha = 45°$, $\varphi = 0$).

5. AXISYMMETRIC V-SHAPED BEARINGS

The V-shaped section has also been investigated for conic bearings applications (Figure 1), with the same geometric dimensions considered for the slide (Figure 5).

5.1. Geometry

For the sake of conciseness, the study of conic bearing has been carried out by considering only two degrees of freedom, e and z (Figure 13). Even for this geometry, a plane analysis, with axial-symmetric option, has been performed for all the cases with eccentricity $e = 0$. A 3D model has been defined for $e \neq 0$; also in this case a simplification can be done, since a plane of symmetry, the one containing the elements axes, still exists (Figure 4).

5.2. Results

The analyses described for the slide geometry have been repeated for the cylindrical bearing. Geometric vectors obtained for the axial-symmetric case are represented in Figure 14, in dimensionless form with respect to a mean tapered area A_m (Figure 13). The trend of the curves can be used for evaluating the behaviour of the force in the four reference magnetization cases.

By comparing diagrams in Figures 7 and 14, that is the slide and the conic bearing, a rather strong similarity can be observed especially for the first two vectors. In Figure 15, a study of the variation of the force with the internal and external magnetisation directions, is shown. Again a similarity with the slide behaviour is evident.

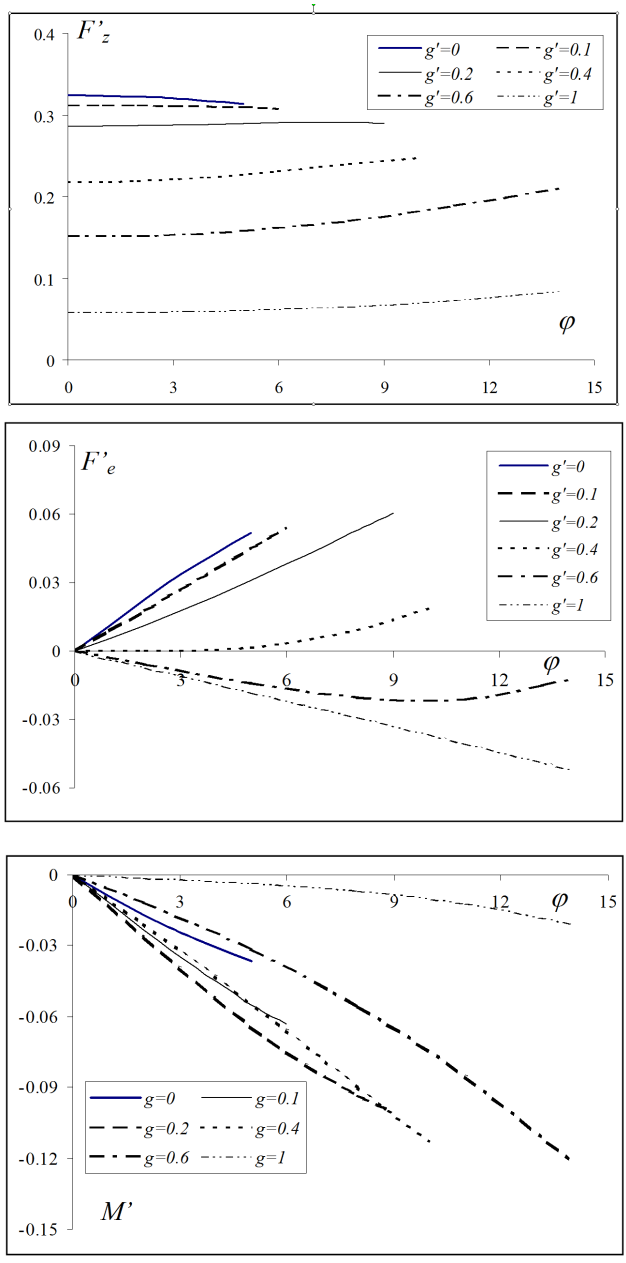

Figure 12. Dimensionless axial and radial forces and moment about point Ω ($\alpha = 45°$, $e = 0$).

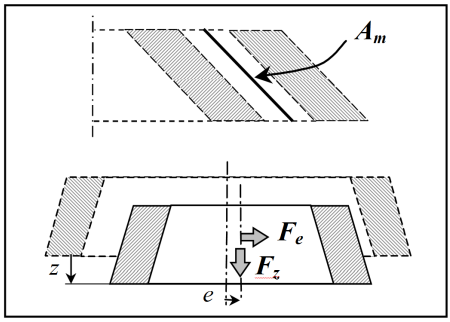

Figure 13. Description of the geometry for a cylindrical bearing.

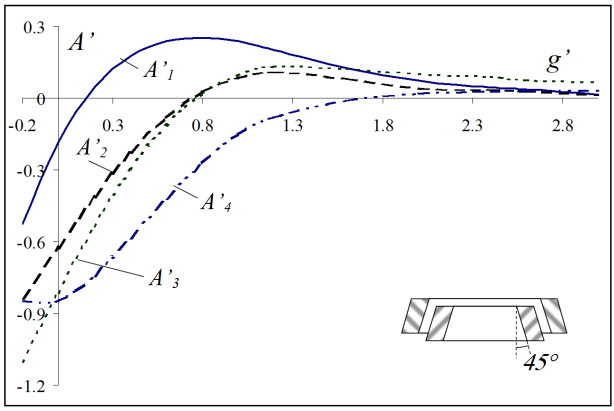

Figure 14. Dimensionless $\mathbf{A}_i$ axial components ($\alpha = 45°$, $e = 0$).

The influence of the angle α on the dimensionless force is shown in Figure 16 as a function of z/h, still for the axial-symmetric problem. The magnetisation is supposed to be parallel to the angle α but with opposite direction in the inner and outer rings. It can be noted that the condition with $\alpha = 0°$ corresponds to an annular bearing with axial magnetization, characterised by zero force in $z = 0$. Conversely, as α grows the conic bearing reaches lower maximum force but in the initial position has a load carrying capacity.

Investigations about the effects of eccentricity have been carried out for axial equiverse magnetisations, as for the slide. Results are reported in Figure 17.

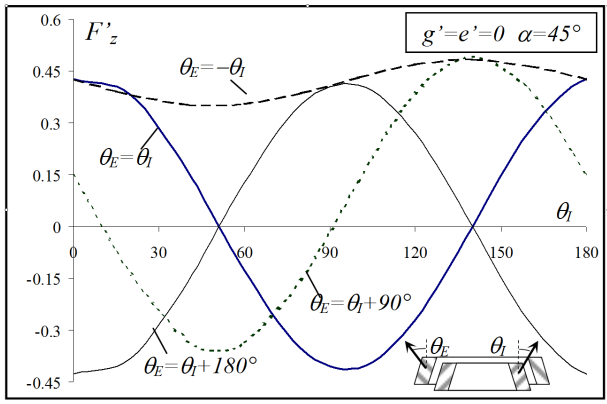

Figure 15. Dimensionless axial force for different bearing angles.

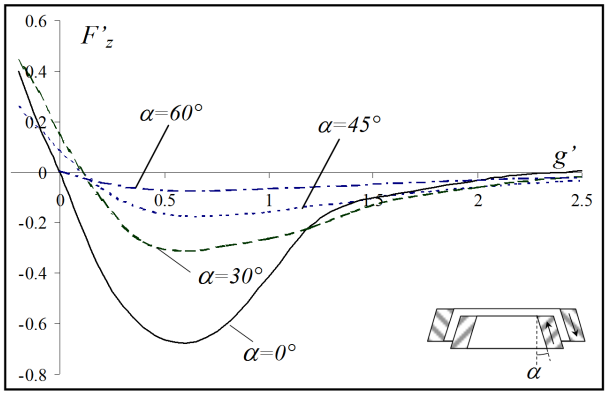

Figure 16. Dimensionless axial force for different bearing angles.

It can be noted that the influence of the eccentricity on the axial component is almost negligible for the range considered as working point ($0 < g' < 0.6$). Moreover, as for the slide, the axial direction is the stable one, while the radial is unstable, in this case the stability condition, because of the axial symmetry, is the following

$$\frac{1}{2}\frac{\partial F_e}{\partial e} + \frac{\partial F_z}{\partial z} = 0 \tag{9}$$

Thus, by comparing (8) and (9), it is evident that the unstable radial force in the cylindrical bearing is nearly a half of that one for

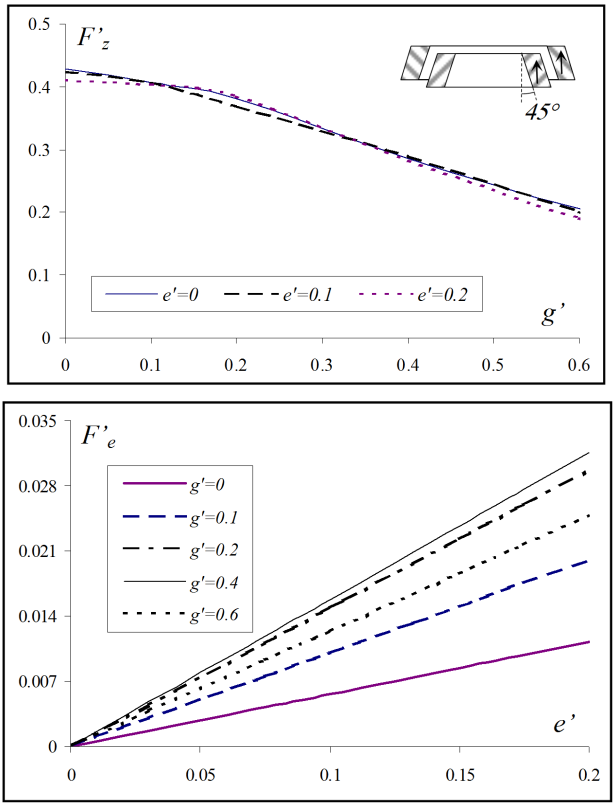

Figure 17. Dimensionless axial and radial forces.

the slide. Due to the many similarities observed between the above described geometries, it is supposed that also the reaction to a rotation for the cylindrical bearing is near to the one described in Figure 12.

6. APPLICATION EXAMPLE

An example of the application of the conic bearing as axial bearings is shown in Figure 18. A shaft carrying a micro-turbine is supported by two bearings arranged in symmetric disposition.

The considered characteristic of the single bearing is the F_z curve vs. g reported in Figure 19(a). In order to avoid any interference in the working conditions, the inner rings of both elements are assembled on the shaft with an initial gap of $g = 0.3\,\text{mm}$. Due to the symmetric position of the bearings, the resultant force F on the shaft is given by

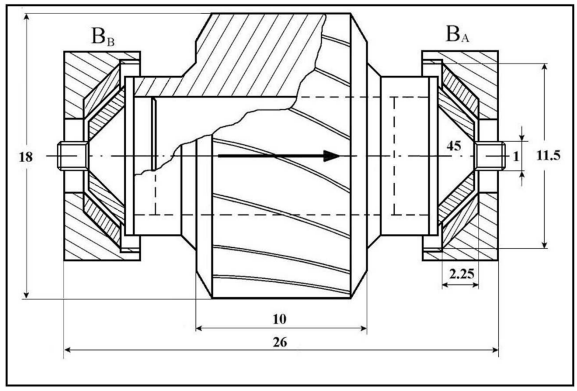

Figure 18. Micro-turbine with conic magnetic bearings; dimensions are expressed in millimeters.

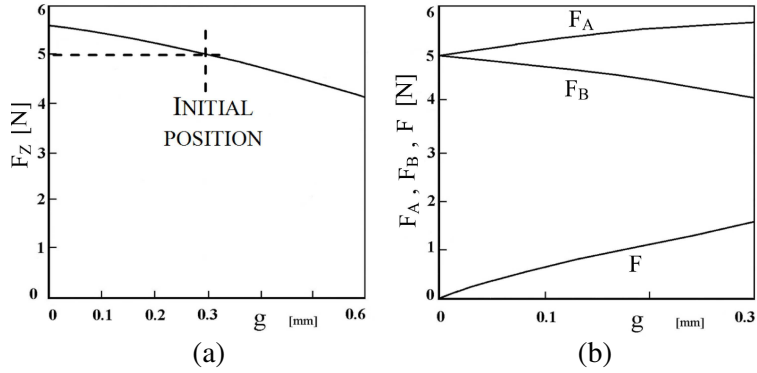

Figure 19. Micro-turbine with conic magnetic bearings. (a) Bearing characteristic; (b) system characteristic: F resulting force, F_A and F_B acting on the bearings B_A and B_B.

the difference of the actions in each bearing, F_A and F_B.

The thrust of the turbine is directed to the right, so the shaft tends to move in that direction, reducing the gap in the B_A bearing and increasing it in the B_B one (see Figure 18). Thus the resultant magnetic reaction on the shaft can be obtained as in Figure 19(b). As already observed for the single bearing, also the double system results unstable in the radial direction. On the other side, the tilting torque observed in Figure 11 for the slide and expected also for the cylindrical bearing is here mainly self-balanced because of the disposition of the elements.

7. CONCLUSIONS

A V-shaped section has been proposed and described for plane slide and conic bearing applications. A method has also been described for designing these elements, considering as parameters the V-half angle α and the directions of the magnetisation vectors. Some results are reported for a reference geometry with $\alpha = 45°$. Investigations of the axial and radial forces have been presented, with some considerations about the stability of the bearing. The presented results can be used for defining permanent magnet bearings with low instability in order to improve the efficiency of the control system. Anyway, it is also possible to study an advantageous combination of magnetic and standard mechanical bearings, the last ones working in the unstable direction and consequently under a rather low force.

As an example, the application of conic bearings to a micro-turbine has been reported, since these devices represent a promising context for future applications of magnetic bearings.

REFERENCES

1. Donald, F., "A passive magnetic-thrust bearing for energy-storage fly wheels," *ASLE Trans.*, Vol. 25, No. 1, 7–16, 1980.
2. Hull, R. J., "Attractive levitation for high-speed ground transport with large guideway clearance and alternating gradient stabilization," *IEEE Trans. Magn.*, Vol. 25, No. 5, 3272–3274, 1989.
3. Jayawant, B. V., *Electromagnetic Levitation and Suspension Systems*, E. J. Arnold, 1981.
4. Parker, J. R., *Advance Permanent Magnetism*, Wiley & Sons, 1990.
5. Fukunaga, H. and Y. Kanai, "Modelling of nano-crystalline magnets using mcromagnetic theory," *Proc. X Int. Congr. Magn.*, 237–250, 1998.
6. Musolino, A., R. Rizzo, M. Tucci, and V. M. Matrosov, "A new passive Maglev system based on eddy current stabilization," *IEEE Trans. Magn.*, Vol. 45, No. 3, 984–987, 2009.
7. Yonnet, J. P., "Permanent magnet bearings and couplings," *IEEE Trans. Magn.*, Vol. 17, No. 1, 1169–1173, 1981.
8. Bassani, R. and S. Villani, "Passive magnetic bearings: The conic-shaped bearing," *Proc. Inst. Mech. Engrs.*, Vol. 213, No. 1, 151–161, 1999.
9. Bekinal, S. I., T. R. Anil, and S. Jana, "Analysis of axially

magnetized permanent magnet bearing characteristics," *Progress In Electromagnetics Research B*, Vol. 44, 327–343, 2012.

10. Babic, S. I. and C. Akyel, "Magnetic force between inclined circular loops (Lorentz approach)," *Progress In Electromagnetics Research B*, Vol. 38, 333–349, 2012.
11. Ausserlechner, U., "Closed analytical formulae for multi-pole magnetic rings," *Progress In Electromagnetics Research B*, Vol. 38, 71–105, 2012.
12. Janssen, J. L. G., J. J. H. Paulides, and E. A. Lomonova, "Study of magnetic gravity compensator topologies using an abstraction in the analytical interaction equations," *Progress In Electromagnetics Research*, Vol. 128, 75–90, 2012.
13. Babic, S. I., C. Akyel, F. Sirois, G. Lemarquand, R. Ravaud, and V. Lemarquand, "Calculation of the mutual inductance and the magnetic force between a thick circular coil of the rectangular cross section and a thin wall solenoid (Integro-Differential approach)," *Progress In Electromagnetics Research B*, Vol. 33, 220–237, 2011.
14. Ravaud, R., G. Lemarquand, and V. Lemarquand, "Halbach structures for permanent magnets bearings," *Progress In Electromagnetic Research M*, Vol. 14, 263–277, 2010.
15. Earnshaw, S., "On the nature of molecular forces which regulate the constitution of luminoferous ether," *Trans. Comb. Phil. Soc.*, Vol. 7, 97–112, 1842.
16. Van der Heide, H., "Stabilization by oscillation," *Philips Tech. Rev.*, Vol. 34, No. 273, 61–72, 1974.
17. Smythe, W. R., *Static and Dynamic Electricity*, Mc Graw Hill, 1959.
18. Barmada, S., A. Musolino, A. Raugi, and R. Rizzo, "Force and torque evaluation in hybrid FEM-MOM formulations," *IEEE Trans. Magn.*, Vol. 37, No. 5, 3108–3111, 2011.
19. Di Puccio, F., "Permanent magnet bearing design: Optimising the magnetisation direction," *Int. Jour. Appl. Mech. and Eng.*, Vol. 9, No. 4, 655–674, 2004.
20. Musolino, A. and R. Rizzo, "Numerical analysis of brush commutation in helical coil electromagnetic launchers," *IET Science, Measurement & Technology*, Vol. 5, No. 4, 147–154, 2011.
21. Musolino, A. and R. Rizzo, "Numerical modeling of helical launchers," *IEEE Trans. Plasma Sci.*, Vol. 39, No. 3, 935–940, 2011.
22. Minciunescu, P., "Contributions to integral equation method for 3D magnetostatic problems," *IEEE Trans. Magn.*, Vol. 34, No. 5,

2461–2464, 1998.

23. Musolino, A., R. Rizzo, E. Tripodi, and M. Toni, "Modeling of electromechanical devices by GPU-accelerated integral formulation," *Int. J. Numer. Model.*, Published online in Wiley Online Library (wileyonlinelibrary.com), 1–21, 2012, DOI:10.1002/jnm.1860.
24. Musolino, A., R. Rizzo, E. Tripodi, and M. Toni, "Acceleration of electromagnetic launchers modeling by using graphic processing unit," *IEEE 16th EML Symposium Conference Proceedings*, 1–6, Beijing, May 15–19, 2012.
25. Barmada, S., A. Musolino, M. Raugi, and R. Rizzo, "Numerical simulation of a complete generator-rail launch system," *IEEE Trans. Magn.*, Vol. 41, No. 1, 369–374, 2005.
26. Barmada, S., A. Musolino, M. Raugi, and R. Rizzo, "Analysis of the performance of a combined coil-rail launcher," *IEEE Trans. Magn.*, Vol. 39, No. 1, 103–107, 2003.
27. Bassani, R., E. Ciulli, F. Di Puccio, and A. Musolino, "Study of conic permanent magnets bearings," *Meccanica*, Vol. 36, No. 6, 745–754, 2001.